JOURNAL OF SPACECRAFT AND ROCKETS
Vol. 38, No. 6, November–December 2001

Dispersion Reduction of a Direct Fire Rocket Using Lateral Pulse Jets

Thanat Jitpraphai* and Mark Costello†
Oregon State University, Corvallis, Oregon 97331

Impact point dispersion of a direct fire rocket can be drastically reduced with a ring of appropriately sized lateral pulse jets coupled to a trajectory tracking flight control system. The system is shown to work well against uncertainty in the form of initial off-axis angular velocity perturbations as well as atmospheric winds. For an example case examined, dispersion was reduced by a factor of 100. Dispersion reduction is a strong function of the number of individual pulse jets, the pulse jet impulse, and the trajectory tracking window size. Proper selection of these parameters for a particular rocket and launcher combination is required to achieve optimum dispersion reduction. For relatively low pulse jet impulse, dispersion steadily decreases as the number of pulse jets is increased or as the pulse jet impulse is increased. For a fixed total pulse jet ring impulse, a single pulse is the optimum pulse jet configuration when the pulse jet ring impulse is small because the effect of a pulse on the trajectory of a rocket decreases as the round flies downrange.

Nomenclature

C_{DD}	=	fin cant roll moment aerodynamic coefficient
C_{LP}	=	roll damping aerodynamic coefficient
C_{MQ}	=	pitch damping aerodynamic coefficient
C_{NA}	=	normal force aerodynamic coefficient
C_{X0}	=	zero yaw axial force aerodynamic coefficient
C_{X2}	=	yaw axial force aerodynamic coefficient
D	=	rocket reference diameter
e_{thres}	=	trajectory tracking window size
L, M, N	=	total applied moments about rocket mass center expressed in the aft body reference frame
n_J	=	number of individual lateral pulse jets
$n_{RX_i}, n_{RY_i}, n_{RZ_i}$	=	ith main rocket motor direction cosines in the body frame
p, q, r	=	components of the angular velocity vector of the projectile in the body reference frame
T	=	$\dot{\gamma}$ time constant
T_{J_i}	=	ith lateral pulse jet thrust
T_{R_i}	=	ith main rocket motor thrust
t^*	=	time of the most recent pulse jet firing
u, v, w	=	components of the velocity vector of the mass center of the composite body in the body reference frame
u_A, v_A, w_A	=	components of the velocity of the mass center of the projectile with mean wind expressed in the body reference frame
V_A	=	magnitude of the velocity vector of the mass center of the projectile experienced with mean wind expressed in the body reference frame
V_{MW}, σ_{MW}	=	magnitude and wind factor of the mean atmospheric wind expressed in the initial reference frame
X, Y, Z	=	total applied force components in the aft body reference frame
x, y, z	=	components of the position vector of center of mass of the composite body in an inertial reference frame
Δ_{PJ}	=	pulse jet firing duration
Δt_{thres}	=	minimum required elapsed time between successive pulse jet firings
δ_{thres}	=	pulse jet angle threshold
θ_i	=	angle between $\boldsymbol{J}_B$ and the ith pulse jet
ρ	=	air density
ϕ, θ, ψ	=	Euler roll, pitch, and yaw angles of the projectile

Received 13 November 2000; presented as Paper 2001-0104 at the 39th Aerospace Sciences Meeting, Reno, NV, 8–11 January 2001; revision received 7 May 2001; accepted for publication 17 May 2001.

*Graduate Research Assistant, Department of Mechanical Engineering. Member AIAA.

†Assistant Professor, Department of Mechanical Engineering. Member AIAA.

Introduction

UNCONTROLLED direct fire rockets exhibit high impact point dispersion, even at relatively short range, and as such have been employed as area weapons on the battlefield. Because direct fire rockets exit the launcher with low velocity, any aerodynamic disturbances presented to the rocket near the launcher create relatively large angles of attack, leading to large aerodynamic jump and increased target dispersion. Furthermore, main rocket motor thrust during the initial portion of flight tends to amplify the effect of initial transverse and angular velocity perturbations on dispersion. The integrated effect over the trajectory of initial disturbances as the rocket enters atmospheric flight and the high sensitivity to atmospheric disturbances lead to large impact point dispersion.

Increased design requirements being placed on direct fire ammunition, including direct fire rockets, call for surgical removal of select targets on the battlefield. Economic realities now stipulate that improved capability be delivered at reduced unit cost. Small, rugged, and inexpensive microelectromechanical sensors coupled to a suitable and inexpensive control mechanism offer the potential to meet these increasingly stringent design requirements. A potential control mechanism that is small, durable, and can be located in close proximity to the sensor suite is a lateral pulse jet ring mounted forward on the rocket body. The pulse jet ring consists of a finite number of individual pulse jets. Each pulse jet on the ring imparts a single, short-duration, large force to the rocket in the plane normal to the rocket axis of symmetry.

The topic of pulse width and pulse frequency modulation has been studied for many years due to applications in the electronics industry. However, most of the resulting control methodologies have been developed for linear or low-order nonlinear systems.[1–6] With regard to spacecraft, Bennighof et al.[7] and Bennighof and Subramaniam[8] demonstrated minimum-time optimal control schemes for flexible structures using pulse response. Singhose et al.[9] proposed fuel-efficient pulse command profiles for flexible spacecraft in which the command profiles consist only of positive or negative constant amplitude impulses. Phillips and Malyevac[10] developed a technique

for pulse motor optimization using mission charts for an exoatmospheric interceptor. The use of lateral pulse jets to improve target dispersion performance of a projectile has been investigated by Harkins and Brown.[11] They used a set of lateral pulse jets to eliminate the off-axis angular rate of the projectile just after exiting the launcher. For the notional concepts considered, dispersion was reduced by a factor of four.

The work reported here seeks to reduce dispersion of an atmospheric rocket using a trajectory tracking flight control system. Pulse jet firing logic is engaged when the trajectory tracking error exceeds a specific threshold. Parametric trade studies that consider the effect of the number of pulse jets, pulse jet impulse, and trajectory tracking window size on impact point dispersion are conducted.

Direct Fire Rocket Dynamic Model

The numerical simulation employed in this study consists of a rigid-body, six-degree-of-freedom model typically utilized in flight dynamic modeling of projectiles. A schematic of the direct fire rocket configuration with major elements of the system identified is given in Fig. 1. The degrees of freedom include three position components of the mass center of the rocket, as well as three Euler orientation angles of the body. The equations of motion are provided in Eqs. (1–4)[12,13]:

$$\begin{Bmatrix}\dot{x}\\ \dot{y}\\ \dot{z}\end{Bmatrix} = \begin{bmatrix} c_\theta c_\psi & s_\phi s_\theta c_\psi - c_\phi s_\psi & c_\phi s_\theta c_\psi + s_\phi s_\psi \\ c_\theta s_\psi & s_\phi s_\theta s_\psi + c_\phi c_\psi & c_\phi s_\theta s_\psi - s_\phi c_\psi \\ -s_\theta & s_\phi c_\theta & c_\phi c_\theta \end{bmatrix} \begin{Bmatrix} u\\ v\\ w\end{Bmatrix} \tag{1}$$

$$\begin{Bmatrix}\dot{\phi}\\ \dot{\theta}\\ \dot{\psi}\end{Bmatrix} = \begin{bmatrix} 1 & s_\phi t_\theta & c_\phi t_\theta \\ 0 & c_\phi & -s_\phi \\ 0 & s_\phi/c_\theta & c_\phi/c_\theta \end{bmatrix} \begin{Bmatrix} p\\ q\\ r\end{Bmatrix} \tag{2}$$

$$\begin{Bmatrix}\dot{u}\\ \dot{v}\\ \dot{w}\end{Bmatrix} = \begin{Bmatrix} X/m\\ Y/m\\ Z/m\end{Bmatrix} - \begin{bmatrix} 0 & -r & q \\ r & 0 & -p \\ -q & p & 0 \end{bmatrix} \begin{Bmatrix} u\\ v\\ w\end{Bmatrix} \tag{3}$$

$$\begin{Bmatrix}\dot{p}\\ \dot{q}\\ \dot{r}\end{Bmatrix} = [I]^{-1}\left[\begin{Bmatrix} L\\ M\\ N\end{Bmatrix} - \begin{bmatrix} 0 & -r & q \\ r & 0 & -p \\ -q & p & 0 \end{bmatrix}[I]\begin{Bmatrix} p\\ q\\ r\end{Bmatrix}\right] \tag{4}$$

The applied loads in Eq. (3) contain contributions from rocket weight W, air loads A, main rocket thrust R, and lateral pulse jet forces J:

$$\begin{Bmatrix} X\\ Y\\ Z\end{Bmatrix} = \begin{Bmatrix} X_W\\ Y_W\\ Z_W\end{Bmatrix} + \begin{Bmatrix} X_A\\ Y_A\\ Z_A\end{Bmatrix} + \begin{Bmatrix} X_R\\ Y_R\\ Z_R\end{Bmatrix} + \begin{Bmatrix} X_J\\ Y_J\\ Z_J\end{Bmatrix} \tag{5}$$

The rocket weight contribution is given by

$$\begin{Bmatrix} X_W\\ Y_W\\ Z_W\end{Bmatrix} = mg\begin{Bmatrix} -s_\theta\\ -s_\phi c_\theta\\ c_\phi c_\theta\end{Bmatrix} \tag{6}$$

whereas the air loads contribution, which acts at the center of pressure of the rocket, is given by

$$\begin{Bmatrix} X_A\\ Y_A\\ Z_A\end{Bmatrix} = -\frac{\pi}{8}\rho V_A^2 D^2 \begin{Bmatrix} C_{X0} + C_{X2}\left(v_A^2 + w_A^2\right)/V_A^2\\ C_{NA}v_A/V_A\\ C_{NA}w_A/V_A\end{Bmatrix} \tag{7}$$

The main rocket motor increases the velocity of the rocket by providing high-thrust levels during the initial portion of the trajectory. In some direct fire rocket designs, the exhaust nozzle contains several flutes such that the exiting flow is turned which causes, in aggregate, a rolling moment. To account for this effect, the numerical simulation models the main rocket motor as a set of four smaller rocket motors that act as point forces on the body. The position and thrust orientation of each small rocket motor on the body are determined to match known inertial properties before and after burn and to match a specified roll time trace. Equation (8) provides the main rocket motor force formula:

$$\begin{Bmatrix} X_R\\ Y_R\\ Z_R\end{Bmatrix} = \sum_{i=1}^{4} T_{Ri}\begin{Bmatrix} n_{RX_i}\\ n_{RY_i}\\ n_{RZ_i}\end{Bmatrix} \tag{8}$$

In Eq. (8), the thrust amplitude profile T_{R_i} is a known function of time. The lateral pulse jet forces are modeled in the same manner as the main rocket motor with two exceptions. Because the lateral pulse jets are active over a very short duration of time when compared to the timescale of a complete rocket trajectory, the thrust force is modeled as a constant when active. Also, because by definition a lateral pulse jet acts in the $\boldsymbol{j}_B$ and $\boldsymbol{k}_B$ plane, the $\boldsymbol{i}_B$ component of the lateral pulse jet force is zero. Equation (9) provides the lateral pulse jet force formula:

$$\begin{Bmatrix} X_J\\ Y_J\\ Z_J\end{Bmatrix} = \sum_{i=1}^{n_J} T_{Ji}\begin{Bmatrix} 0\\ -\cos[2\pi(i-1)/n_J]\\ -\sin[2\pi(i-1)/n_J]\end{Bmatrix} \tag{9}$$

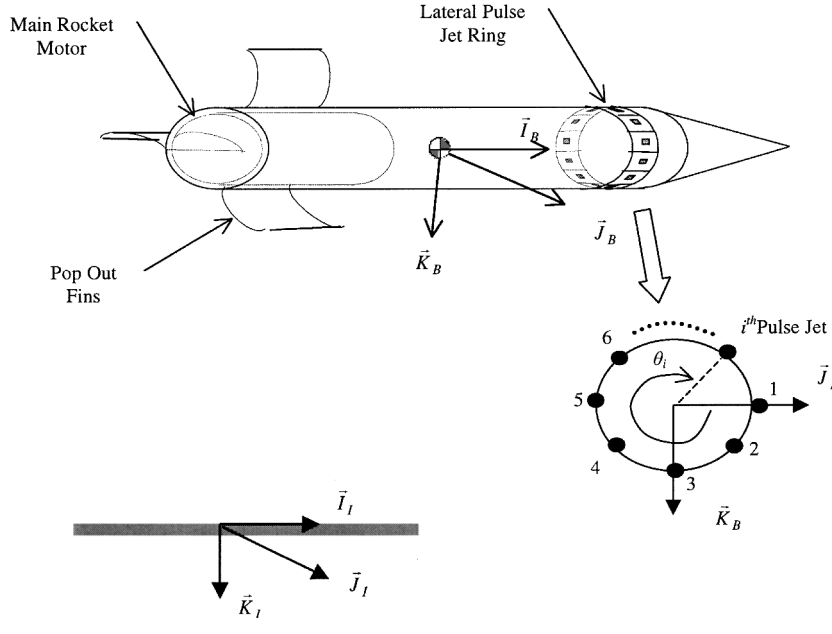

Fig. 1 Schematic of a direct fire rocket with lateral pulse jets.

The pulse jet ring is located on the skin of the projectile and near the nose of the rocket. Individual pulse jets are uniformly distributed azimuthally around the lateral pulse jet ring. A key feature of the pulse jet configuration considered here is that each pulse jet can be fired only once.

The applied moments about the rocket mass center contains contributions from steady air loads SA, unsteady air loads UA, main rocket thrust R, and lateral pulse jet forces J:

$$\begin{Bmatrix} L \\ M \\ N \end{Bmatrix} = \begin{Bmatrix} L_{SA} \\ M_{SA} \\ N_{SA} \end{Bmatrix} + \begin{Bmatrix} L_{UA} \\ M_{UA} \\ N_{UA} \end{Bmatrix} + \begin{Bmatrix} L_R \\ M_R \\ N_R \end{Bmatrix} + \begin{Bmatrix} L_J \\ M_J \\ N_J \end{Bmatrix} \tag{10}$$

The moment components due to steady aerodynamic forces, main rocket motor forces, and lateral pulse jet forces are computed with a cross product between the distance vector from the mass center of the rocket and the location of the specific force and the force itself. The unsteady body aerodynamic moment provides a damping source for projectile angular motion and is given by

$$\begin{Bmatrix} L_{UA} \\ M_{UA} \\ N_{UA} \end{Bmatrix} = \frac{\pi}{8}\rho V_A^2 D^3 \begin{Bmatrix} C_{DD} + \dfrac{pDC_{LP}}{2V_A} \\ \dfrac{qDC_{MQ}}{2V_A} \\ \dfrac{rDC_{MQ}}{2V_A} \end{Bmatrix} \tag{11}$$

When the rocket motors are active, the mass, mass center location, and inertial properties of the rocket are updated continuously. The center of pressure location and all aerodynamic coefficients depend on local Mach number. The air velocity of the mass center of the rocket includes contributions from inertial motion of the round and atmospheric mean wind. The mean atmospheric wind acts in the horizontal plane and is directed at an angle ψ_{MW} from the $\boldsymbol{i}_I$ axis:

$$\begin{Bmatrix} u_A \\ v_A \\ w_A \end{Bmatrix} = \begin{Bmatrix} u \\ v \\ w \end{Bmatrix} + \begin{bmatrix} c_\theta c_\psi & c_\theta s_\psi & -s_\theta \\ s_\phi s_\theta c_\psi - c_\phi s_\psi & s_\phi s_\theta s_\psi + c_\phi c_\psi & s_\phi c_\theta \\ c_\phi s_\theta c_\psi + s_\phi s_\psi & c_\phi s_\theta s_\psi - s_\phi c_\psi & s_\phi c_\theta \end{bmatrix} \times \begin{Bmatrix} V_{MW} c_{\psi_{MW}} \\ V_{MW} s_{\psi_{MW}} \\ 0 \end{Bmatrix} \tag{12}$$

A representative mean wind speed that increases with altitude to a limiting value of σ_{MW} is

$$V_{MW} = 0.636619\sigma_{MW} \tan^{-1}(|z|/1000) \tag{13}$$

Direct Fire Rocket Flight Control System

The flight control system seeks to track a prespecified command trajectory utilizing the control authority provided by the lateral pulse jets. A schematic of the flight control system block diagram is shown in Fig. 2, and a schematic of the lateral pulse jet firing logic is given in Fig. 3. For direct fire rockets, a command ballistic trajectory is available from the fire control system and can be downloaded to the round just before launch. The trajectory tracking flight control system first compares the measured position of the projectile to the commanded trajectory to form a position error vector in the inertial frame. Position and orientation sensor feedback is assumed to be perfect, that is, not corrupted by noise, bias, or cross axis sensitivity. The trajectory error is converted to the rocket body frame using

$$\begin{Bmatrix} e_X \\ e_Y \\ e_Z \end{Bmatrix} = \begin{bmatrix} c_\theta c_\psi & c_\theta s_\psi & -s_\theta \\ s_\phi s_\theta c_\psi - c_\phi s_\psi & s_\phi s_\theta s_\psi + c_\phi c_\psi & s_\phi c_\theta \\ c_\phi s_\theta c_\psi + s_\phi s_\psi & c_\phi s_\theta s_\psi - s_\phi c_\psi & c_\phi c_\theta \end{bmatrix} \begin{Bmatrix} x_C - x \\ y_C - y \\ z_C - z \end{Bmatrix} \tag{14}$$

The magnitude and phase of the error in the off-axis plane of the rocket are Γ and γ, and are defined by, respectively,

$$\Gamma = \sqrt{e_Y^2 + e_Z^2} \tag{15}$$

$$\gamma = \tan^{-1}(e_Z/e_Y) \tag{16}$$

At each computation cycle in the flight control system, a sequence of checks are conducted that govern firing of individual lateral pulse jets. The conditions that must be satisfied for an individual lateral pulse jet to fire are as follows:

1) Magnitude of the off-axis trajectory tracking error must be greater than a specified distance:

$$\Gamma > e_{\text{thres}} \tag{17}$$

2) Time elapsed since the last lateral pulse jet firing must be greater than a specified duration:

$$t - t^* > \Delta t_{\text{thres}} \tag{18}$$

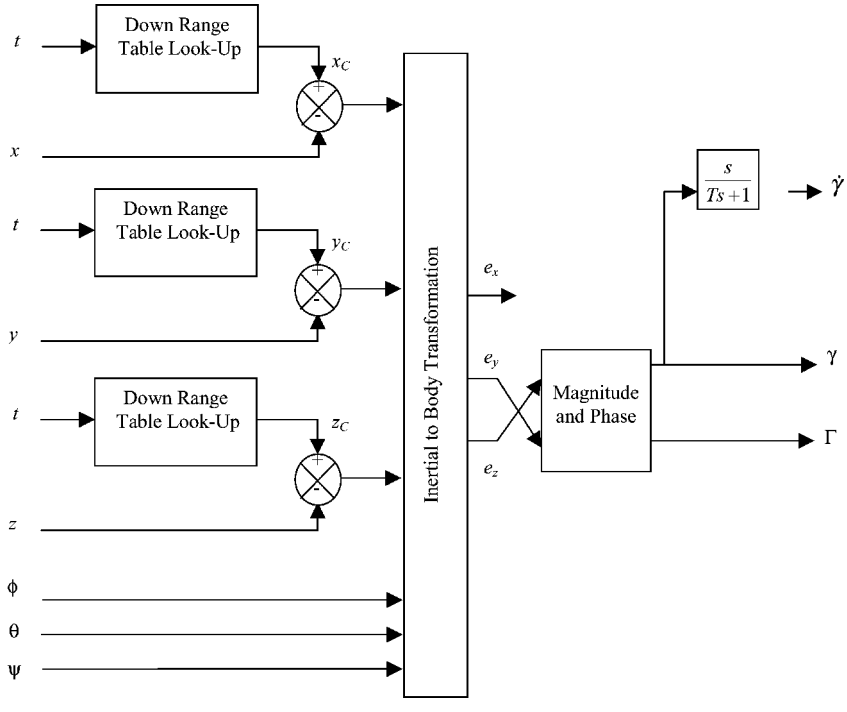

Fig. 2 Trajectory tracking flight control system.

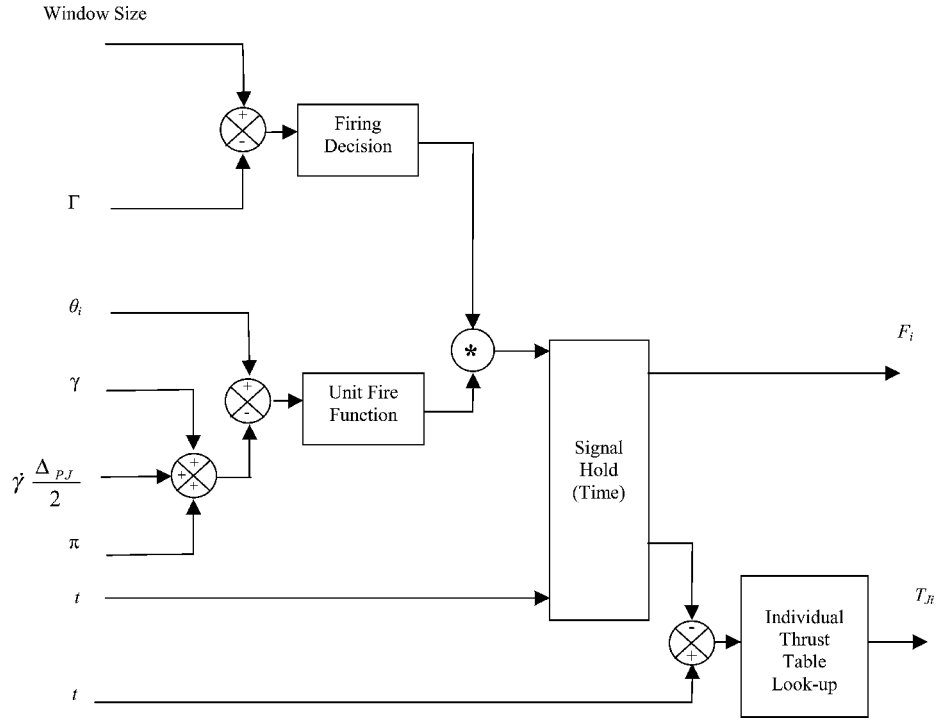

Fig. 3 Diagram of *i*th individual lateral pulse jet firing logic.

3) Projected angle between the trajectory tracking error and the individual pulse jet force under consideration is less than a specified angle:

$$|\theta_i - \pi - \gamma - \dot{\gamma}(\Delta_{\mathrm{PJ}}/2)| < \delta_{\mathrm{thres}} \tag{19}$$

4) The individual pulse jet under consideration has not been fired. The first two checks are valid for all lateral pulse jets, whereas the last two checks are specific to a given lateral pulse jet. The flight control system contains only three parameters that must be tuned to a specific application, namely, the tracking error window size, the required elapsed time between pulse jet firings, and the angle tolerance between the tracking error and the individual pulse jet force.

Results

To investigate the ability of a lateral pulse jet ring to reduce impact point dispersion, the equations of motion described earlier are numerically integrated using a fourth-order Runge–Kutta algorithm. The rocket configuration used in the simulation study is a representative direct fire rocket that is a 1.4-m-long, fin-stabilized rocket with three popout fins on the rear of the round. The lateral pulse jet ring is located 1.16 m from the base of the rocket. The main rocket motor burns for 1.12 s and imparts an impulse to the rocket of 6212 N-s. During the main rocket motor burn, the forward velocity of the rocket is increased from 43.7 to 767.5 m/s. The rocket weight, mass center location from the base of the rocket, roll inertia, and pitch inertia before and after burn is 10.4/7.21 kg, 0.85/0.86 m, 0.0077/0.0058 kg · m^2, and 1.83/1.61 kg · m^2, respectively. Nominally, the rocket exits the launcher with the following initial conditions: $x = 0.0$ m, $y = 0.0$ m, $z = -30.5$ m, $\phi = 0.0$ deg, $\theta = 4.14$ deg, $\psi = 0.0$ deg, $u = 43.7$ m/s, $v = 0.0$ m/s, $w = 0.11$ m/s, $p = 51.5$ rad/s, $q = -0.18$ rad/s, and $r = 0.0$ rad/s.

Figures 4–11 compare uncontrolled and controlled trajectories for the example rocket configuration against a nominal command trajectory. The nominal command trajectory is the trajectory the projectile seeks to track. This trajectory is uploaded to the projectile just before launch from the weapon platform. The uncontrolled trajectory is the projectile trajectory when no pulse jets are fired and the initial angular rates are introduced to model launcher vibration. The ring contains 32 individual lateral pulse jets, where each individual pulse jet imparts an impulse of 5 N-s on the projectile body over a time duration of 0.001 s. The rocket is launched at an altitude of 30 m toward a target on the ground with altitude and cross range equal zero at a range of 3000 m. The trajectory tracking window size

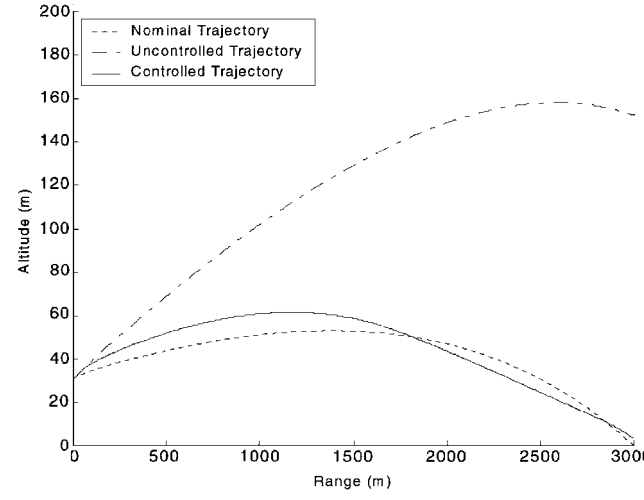

Fig. 4 Altitude vs range.

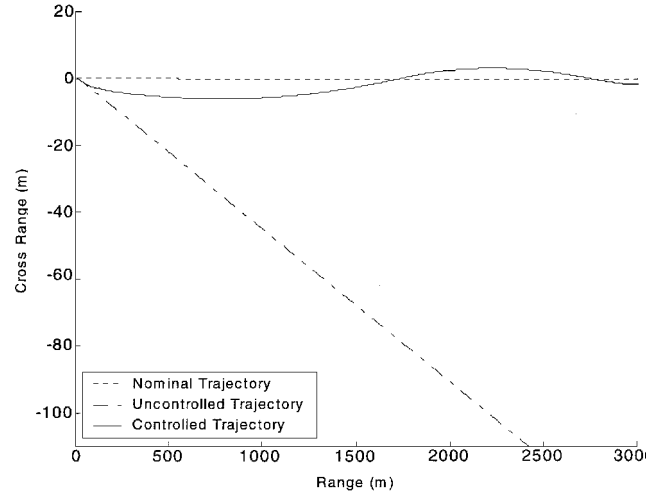

Fig. 5 Cross range vs range.

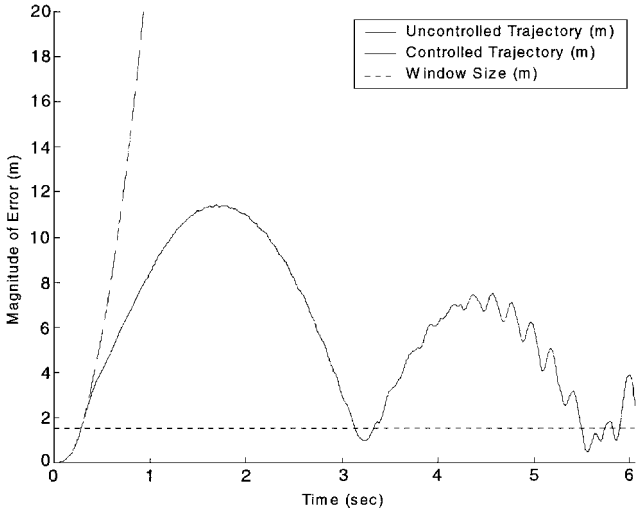

Fig. 6 Trajectory tracking error vs time.

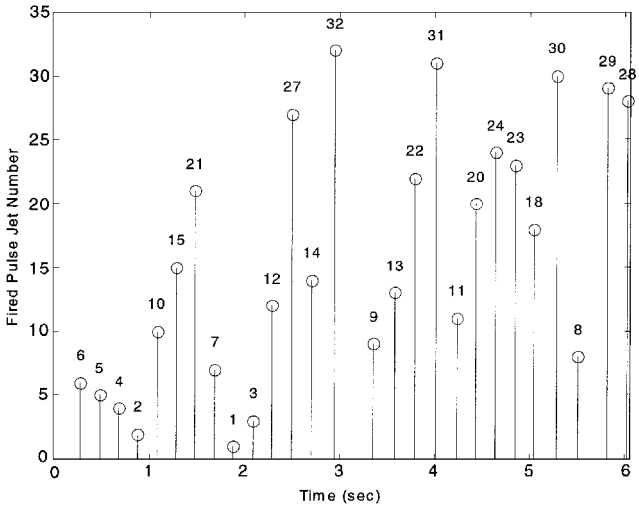

Fig. 7 Pulse jet firing time

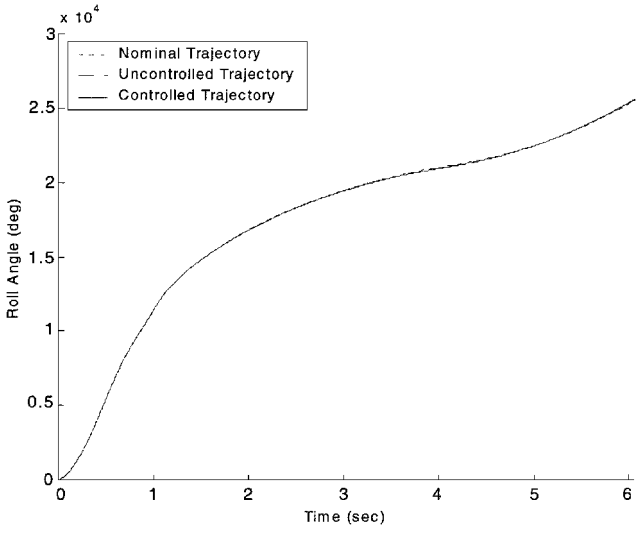

Fig. 8 Roll angle vs time.

is set to 1.5 m, and the pulse jet elapsed time threshold is set to 0.2 s. The pulse jet angle threshold is set to 0.1 deg. Figures 4 and 5 plot rocket altitude and cross range vs range. At the target range of 3000 m, the uncontrolled rocket altitude error is slightly greater than 110 m, and the cross range error is more than 100 m. Compared to the uncontrolled trajectory, the controlled rocket trajectory follows the commanded trajectory well with an impact error on the order of several meters.

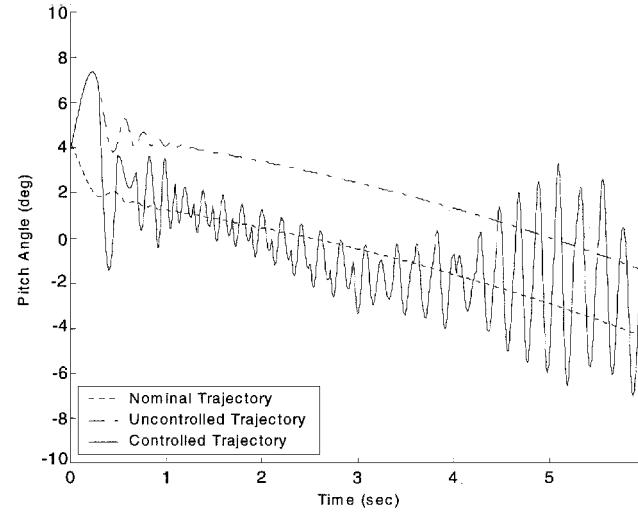

Fig. 9 Euler pitch angle vs time.

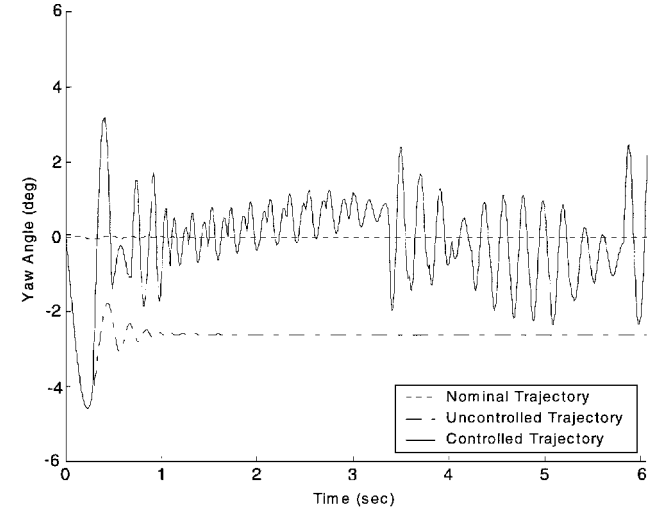

Fig. 10 Euler yaw angle vs time.

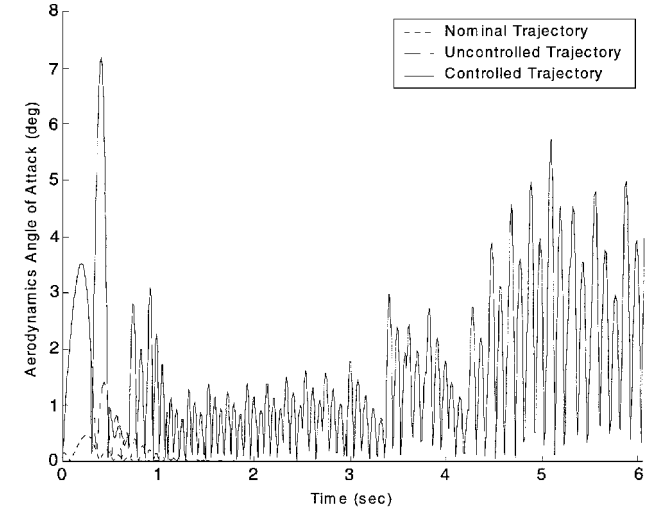

Fig. 11 Aerodynamic angle of attack vs time.

The off-axis trajectory tracking error Γ is plotted in Fig. 6. Although the uncontrolled rocket trajectory error is greater than 100 m, the trajectory tracking error for the lateral pulse jet controlled rocket remains under 12 m for the entire flight. The sequence of lateral pulse jet firing times is shown in Fig. 7. After each individual pulse jet is fired, a time interval of Δt_{thres} must elapse before another jet is fired. For a time of flight to the target, $t_{\max}$, the maximum number of pulse jets that can be fired to reduced impact error is $t_{\max}/\Delta t_{\text{thres}}$.

Of the possible 32 lateral pulse jets, 27 are fired in this particular example. Notice that pulses are fired at a maximum rate of 1 firing per 0.2 s. The minimum required time between successive pulses, Δt_{thres}, is an important design parameter of the flight control system. If Δt_{thres} is set too low, the rocket does not have sufficient time to respond, and many pulses will be fired, tending to overcompensate for trajectory errors. On the other hand, if Δt_{thres} is set too high, then only a small number of pulses can possibly be fired, and control authority is wasted. In this instance, trajectory tracking error will tend to build without pulse jet corrective action.

The roll angle time history is shown in Fig. 8, and it is seen that the roll response is essentially unaffected by the action of the lateral pulse jets because both the controlled and uncontrolled roll angle time histories are approximately equal. A comparison of pitch attitude for the uncontrolled and controlled trajectories is provided in Fig. 9. Whereas the nominal and uncontrolled trajectories show a steady decrease in pitch attitude as the rocket flies downrange, the controlled trajectory shows oscillatory response due to the firing of pulse jets. Total pitch angle excursions of greater than 10 deg are experienced toward the end of the trajectory. Similar oscillations are seen in the yaw angle time history shown in Fig. 10. The approximate difference of 2 deg in the steady-state Euler pitch and yaw angles between the nominal and uncontrolled trajectories is an indicator of aerodynamic jump caused by the difference in initial angular rates. The aerodynamic angle of attack of the nominal, uncontrolled, and controlled cases are shown in Fig. 11. Whereas the angle of attack for the nominal and uncontrolled cases remains relatively small and under 2.5 deg, the action of pulse jets induces angles of attack greater than 7 deg near the target.

The initial state of the rocket as it exits the launcher and enters free flight can be viewed as a random process. The random nature of the initial free-flight state stems from many effects but perhaps most notably from launcher and rocket manufacturing tolerances combined with resulting launcher and rocket vibration. Random perturbations in initial free-flight conditions creates target dispersion. Furthermore, for direct fire rockets, perturbations in initial off-axis angular rates have been found to significantly contribute to the impact point error budget.[14,15] Figure 12 compares impact points at a range of 3000 m for the uncontrolled and controlled direct fire rocket configurations with a sample size of 75, where the initial pitch rate and yaw rate are independent Gaussian random variables. The mean value for pitch and yaw rate is −0.18 and 0 rad/s, respectively. The standard deviation for both pitch and yaw rate is 0.3 rad/s. The dispersion radius is defined as the radius of a circle that emanates from the mean impact point and contains 67% of the impact points. The large circle in Fig. 12 is the dispersion radius for the uncontrolled case, which is equal to 106.8 m, whereas the dispersion radius for the controlled case is 1.4 m and is not noticeable in Fig. 12.

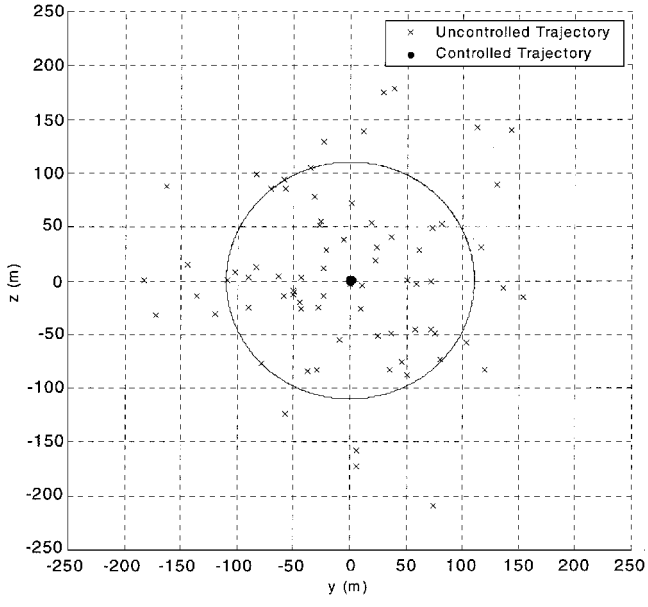

Fig. 12 Impact point dispersion (perturbed initial pitch and yaw rate).

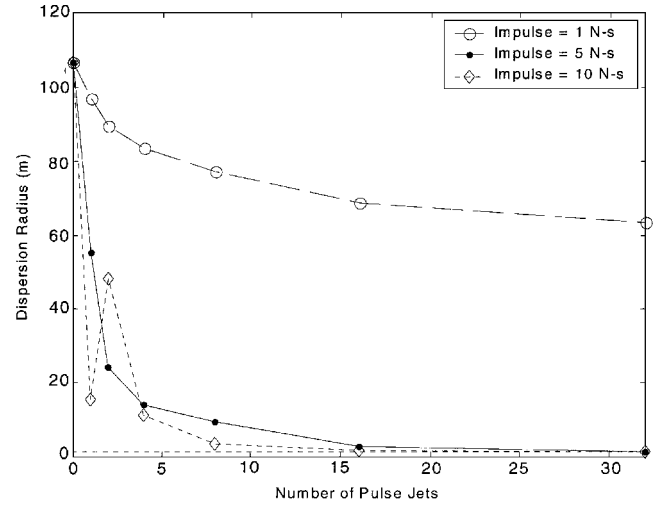

Fig. 13 Dispersion radius vs number of pulse jets and pulse jet impulse (trajectory tracking window size = 1.5 m).

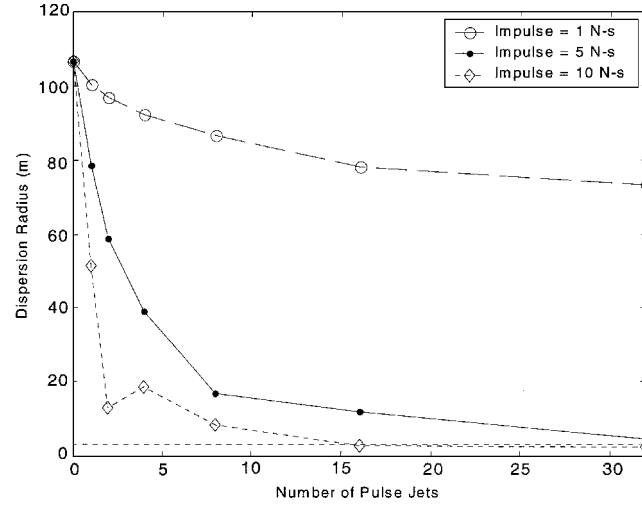

Fig. 14 Dispersion radius vs number of pulse jets and pulse jet impulse (trajectory tracking window size = 3.0 m).

Figures 13–15 show the relationship between dispersion radius, number of pulse jets on the ring, and individual pulse jet impulse for three different trajectory tracking window sizes of 1.5, 3.0, and 4.5 m. As the number of individual pulse jets is increased, the total impulse contained in the pulse jet ring is increased. In each graph, the trajectory tracking window size is shown as a constant dashed line. When the impulse for the individual lateral pulse jets is small, dispersion radius is steadily reduced as the number of pulse jets or the jet impulse is increased. When Figs. 13–15 are viewed, it is seen that the 1-N-s impulse is underpowered for the rocket. When the individual lateral pulse jet impulse is relatively large, adding more pulse jets can actually increase the dispersion radius. For a small tracking window size and large impulse, the dispersion radius oscillates as the total number of jets is increased. In this case, the lateral pulse jet impulse is so large compared to the trajectory tracking error that firing a particular pulse jet tends to overcorrect the tracking error leading to larger target dispersion. In these cases, the pulse jets are overpowered for the tracking error they seek to maintain. When Figs. 13–15 are contrasted for a given pulse jet configuration, dispersion is generally reduced as the tracking window size is reduced. The exception to this rule is high-impulse jets, which do not show a definite trend due to the overshoot problem mentioned earlier.

Figure 16 shows the relationship between dispersion radius, number of pulse jets on the ring, and the total ring impulse for a trajectory tracking window size of 1.5 m. Each line in Fig. 16 represents lines of constant total ring impulse. For these traces, as the number of lateral pulse jets on the ring is increased, the impulse for an individual lateral pulse jet decreases proportionally so that the

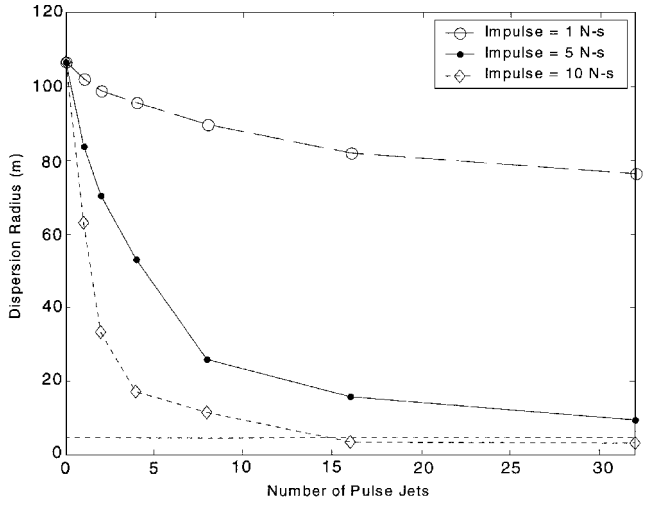

Fig. 15 Dispersion radius vs number of pulse jets and pulse jet impulse (trajectory tracking window size = 4.5 m).

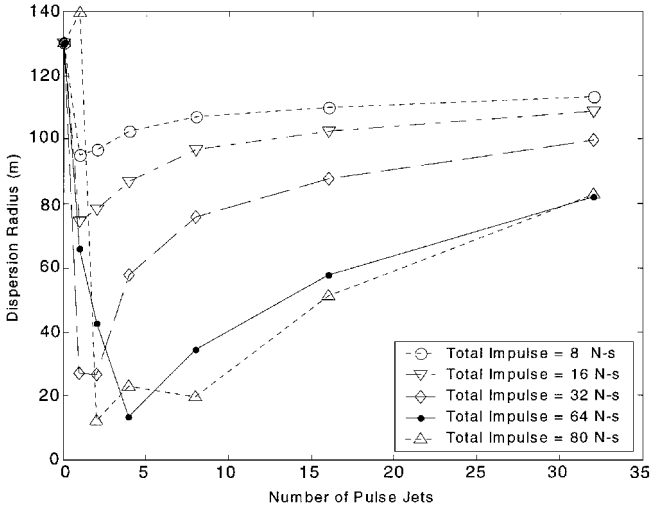

Fig. 16 Dispersion radius vs number of pulse jets and total ring impulse (trajectory tracking window size = 3.0 m).

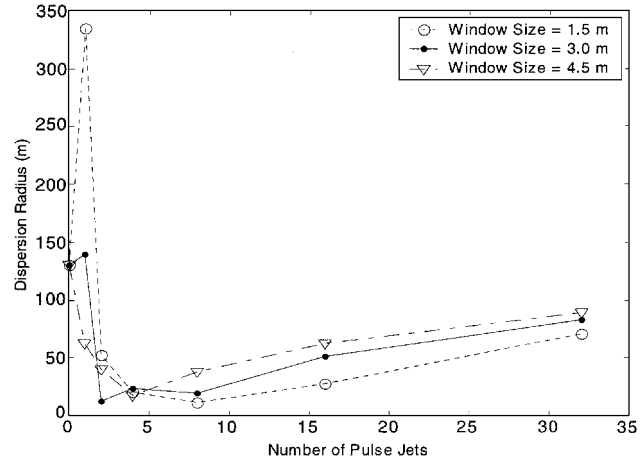

Fig. 17 Dispersion radius vs number of pulse jets and trajectory tracking window size (total ring impulse = 80 N-s).

total ring impulse remains constant. For relatively low total ring impulse, a single lateral pulse jet yields the lowest dispersion radius. The reason for this trend is that the effectiveness of a pulse jet on the trajectory decreases sharply as the projectile flies downrange. Hence, a comparatively large and early trajectory correction provides more of an impact point modification than two pulses, each of half impulse strength, where one of the pulses occurs farther downrange. As the total impulse on the ring is increased, the minimum dispersion radius is decreased. For relatively large total ring impulse, an optimum number of individual lateral pulse jets exists for a given trajectory tracking window size. In the example shown in Fig. 16, a total ring impulse of 64 N-s split into four individual lateral pulse jets provides the optimum dispersion reduction. Figure 17 plots the dispersion radius vs the number of pulse jets for three different trajectory tracking window sizes. The total ring impulse for all data on the chart is 80 N-s. A single impulse increases the dispersion radius for trajectory tracking window sizes of 1.5 and 3.0 m. Figure 17 underlines the importance of properly selecting the number of pulse jets and the pulse jet impulse for a particular accuracy design requirement.

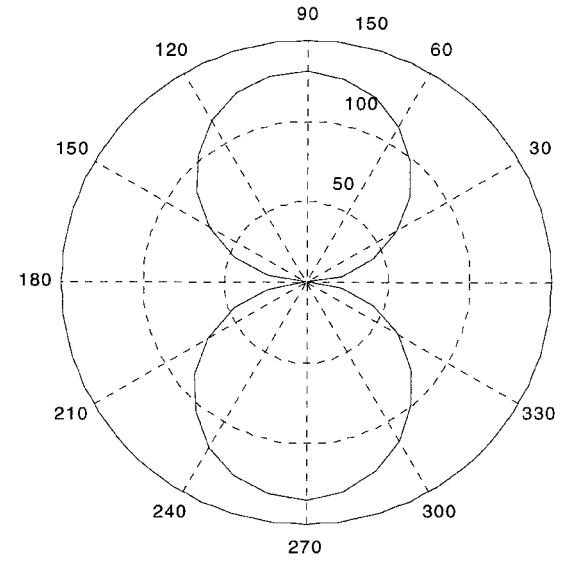

Fig. 18 Dispersion radius vs atmospheric wind direction for the uncontrolled rocket (atmospheric wind speed = 7.6 m/s, number of pulse jets = 32, pulse jet impulse = 20 N-s, and trajectory tracking window size = 1.5 m).

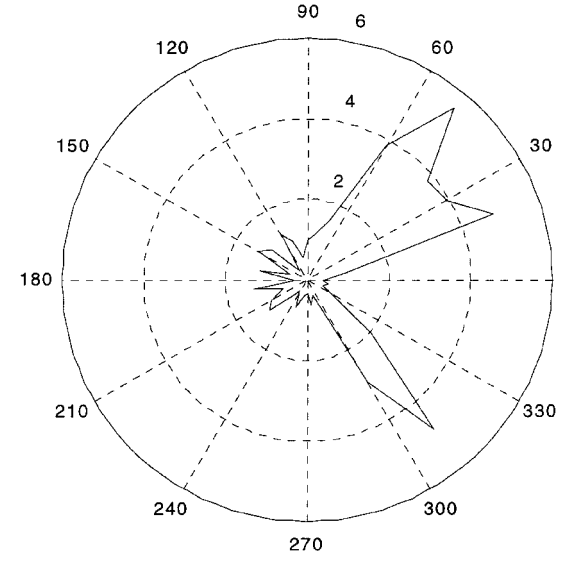

Fig. 19 Dispersion radius vs atmospheric wind direction for the controlled rocket (atmospheric wind speed = 7.6 m/s, number of pulse jets = 32, pulse jet impulse = 20 N-s, and trajectory tracking window size = 1.5 m).

Figures 18 and 19 plot dispersion radius as a function of the atmospheric wind angle for the uncontrolled and controlled rocket configurations, respectively. An atmospheric wind angle of 0 deg corresponds to a direct head wind, whereas an angle of 180 deg represents a direct tail wind. The uncontrolled rocket configuration is insensitive to direct head and tail winds because in these cases the rocket range is predominantly effected. On the other hand, side

winds induce dispersion over 130 m. The controlled rocket configuration successfully suppresses dispersion to under 6 m for all wind directions.

Conclusions

Using a previously validated, six-degree-of-freedom dynamic model of a direct fire rocket, a drastic reduction in impact point dispersion using a lateral pulse jet control mechanism coupled to a trajectory tracking flight control system is demonstrated. The ability to improve dispersion performance must be weighed against the cost of installing an inertial measurement unit sensor suite and a pulse jet ring onboard existing unguided direct fire rockets. In designing a lateral pulse jet control system, the number of pulse jets and the pulse jet impulse must be carefully tuned against the desired impact point dispersion and the level of uncertainty within the rocket.

References

[1]Pavlidis, T., "Optimal Control of Pulse Frequency Modulated Systems," *IEEE Transactions on Automatic Control*, Vol. AC-11, No. 1, 1966, pp. 676–684.

[2]Onyshko, S., and Noges, E., "Optimization of Pulse Frequency Modulated Control Systems via Modified Maximum Principle," *IEEE Transactions on Automatic Control*, Vol. AC-13, No. 2, 1968, pp. 144–149.

[3]VanderStoep, D., and Alexandro, F., "Bounds on the Optimal Performance of Pulse Controlled Linear Systems," *IEEE Transactions on Automatic Control*, Vol. AC-13, No. 1, 1968, pp. 88–90.

[4]Nicoletti, B., and Raiconi, G., "A Computer Algorithm for the Optimization of Discrete Time Pulse Frequency Modulated Systems," *IEEE Transactions on Automatic Control*, Vol. AC-19, No. 4, 1974, pp. 407–410.

[5]Onyshko, S., and Noges, E., "Pulse Frequency Modulation and Dynamic Programming," *IEEE Transactions on Automatic Control*, Vol. AC-14, No. 5, 1969, pp. 558–561.

[6]Elgazzar, S., and Onyshko, S., "Optimal Control Computation in Pulse Frequency Modulated Control Systems," *IEEE Transactions on Automatic Control*, Vol. AC-19, No. 4, 1974, pp. 452–454.

[7]Bennighof, J., Chang, S., and Subramaniam, M., "Minimum Time Pulse Response Based Control of Flexible Structures," *Journal of Guidance, Control, and Dynamics*, Vol. 16, No. 5, 1993, pp. 874–882.

[8]Bennighof, J. K., and Subramaniam, M., "Minimum Time Maneuver of Flexible Systems Using Pulse Response Based Control," *Journal of Guidance, Control, and Dynamics*, Vol. 20, No. 1, 1997, pp. 129–136.

[9]Singhose, W., Bohlke, K., and Seering, W., "Fuel-Efficient Pulse Command Profiles for Flexible Spacecraft," *Journal of Guidance, Control, and Dynamics*, Vol. 19, No. 4, 1996, pp. 954–960.

[10]Phillips, C., and Malyevac, D., "Pulse Motor Optimization via Mission Charts for an Exoatmospheric Interceptor," *Journal of Guidance, Control, and Dynamics*, Vol. 21, No. 4, 1998, pp. 611–617.

[11]Harkins, T. E., and Brown, T. G., "Using Active Damping as a Precision-Enhancing Technology for 2.75-Inch Rockets," U.S. Army Research Lab., ARL TR-1772, Aberdeen Proving Ground, MD, 1999.

[12]Gast, R., Morris, S., and Costello, M., "Simulation of Shot Impacts for the M1A1 Tank Gun," *Journal of Guidance, Control, and Dynamics*, Vol. 23, No. 1, 2000, pp. 53–59.

[13]Costello, M., and Anderson, D., "Effect of Internal Mass Unbalance on the Terminal Accuracy and Stability of a Projectile," *Proceedings of the AIAA Flight Mechanics Conference*, AIAA, Reston, VA, 1996.

[14]Carter, R., Chase, W., and Whiteside, J., "Accuracy Analysis for the Advanced Rocket System," U.S. Army Research, Development, and Engineering Center, Rept. FTB-IR-14, Picatinny Arsenal, NJ, 1994.

[15]Bellamy, R., Chase, W., and Whiteside, J., "Accuracy Analysis for the 2.75-inch MK66 Rocket," U.S. Army Research, Development, and Engineering Center, Rept. FTB-IR-23, Picatinny Arsenal, NJ, 1995.

P. Weinacht
Associate Editor